AIP | Physics of Fluids

Numerical simulation of the settling behaviour of particles in thixotropic fluids

M. M. Gumulya, R. R. Horsley, and V. Pareek

Citation: Physics of Fluids **26**, 023102 (2014); doi: 10.1063/1.4866320
View online: http://dx.doi.org/10.1063/1.4866320
View Table of Contents: http://scitation.aip.org/content/aip/journal/pof2/26/2?ver=pdfcov
Published by the AIP Publishing

PHYSICS OF FLUIDS **26**, 023102 (2014)

Numerical simulation of the settling behaviour of particles in thixotropic fluids

M. M. Gumulya, R. R. Horsley,[a] and V. Pareek
Department of Chemical Engineering, Curtin University, U1987, Perth, WA 6845, Australia

(Received 16 April 2013; accepted 7 February 2014; published online 25 February 2014)

A numerical study on the settling behaviour of particles in shear–thinning thixotropic fluids has been conducted. The numerical scheme was based on the volume of fluid model, with the solid particle being likened to a fluid with very high viscosity. The validity of this model was confirmed through comparisons of the flow field surrounding a sphere settling in a Newtonian fluid with the analytical results of Stokes. The rheology model for the fluid was time–dependent, utilising a scalar parameter that represents the integrity of a "structural network," which determines its shear thinning and thixotropic characteristics. The results of this study show that the flow field surrounding the settling sphere is highly localised, with distinct regions of disturbed/undisturbed fluids. The extension of these regions depends on the relaxation time of the fluid, as well as its shear thinning characteristics, and reflects the drag force experienced by the sphere. As the sphere settles, a region of sheared fluid that has significantly lower values of viscosity is formed above the sphere. This region slowly recovers in structure in time. As a result, a sphere that falls in a partially recovered domain (e.g., due to the shearing motion of an earlier sphere) tends to attain a greater velocity than the terminal velocity value. This was found to be true even in cases where the "resting time" of the fluid was nearly twice the relaxation time of the fluid. The results of this study could provide a framework for future analysis on the time–dependent settling behaviour of particles in thixotropic shear–thinning fluids. © *2014 AIP Publishing LLC*. [http://dx.doi.org/10.1063/1.4866320]

I. INTRODUCTION

Suspensions of fine mineral particles that are encountered in the mineral processing industry generally possess non–Newtonian flow characteristics, usually in the form of viscoplasticity, thixotropy, and/or shear thinning flow behaviour, or various combinations of these characteristics. As can be expected, the settling behaviour of particles suspended in slurries and suspensions is greatly dependent on the rheology of the suspending fluids (Ref. 1). In turn, the design and performance of many slurry based units of operations, most notably the tertiary grinding circuits, are highly influenced by the tendency of suspended particles to settle and fall through the suspension. Therefore, to improve the efficiency of these units of operations, a greater understanding of the movement of particles through suspensions and slurries needs to be obtained.

The settling behaviour of particles in viscous fluids has been examined extensively by Gumulya *et al.*,[2,3] using solutions of polyacrylamide in water. These solutions were identified as highly shear thinning with thixotropic characteristics. Under short timescales, the existence of a critical value of shear stress that has to be exceeded for the fluid to start to flow (generally termed as yield stress) is apparent, indicating that the fluids can be represented by a simple viscoplastic fluid model. However, in cases where longer time frames are involved (e.g., in experiments involving the settling of consecutive particles with a finite time lapse between them (Refs. 2 and 3)), it was found that both the thixotropic and shear thinning characteristics of the materials need to be considered.

[a]Deceased.

Gumulya *et al.*[2,3] observed that a sphere that is released into a fluid medium that has recently been subjected to shear tends to possess a settling velocity that is significantly higher than a sphere that is settling through a fluid medium that has been rested for some time. This finding suggests that the settling motion of a sphere through the fluid introduces changes in the structure of the fluid (it was hypothesised that this network results from hydrogen bonding between polyacrylamide and water molecules in the fluid), which in turn requires some "resting" time for its full recovery. It was thus concluded that the analysis of the settling behaviour of particles through complex fluids requires the shear induced changes in the internal structures of the fluids to be characterised.

While various studies have been conducted on the characterisation of the flow field surrounding particles settling in yield stress fluids (Refs. 4–8), such studies on shear thinning, thixotropic fluids are still very scarce, despite the fact that some yield stress fluids are known to possess a combination of all these characteristics. Gueslin *et al.*[9,10] and Putz *et al.*[11] have conducted flow–visualisation experiments on the flow surrounding spheres settling in thixotropic yield stress fluids with viscoelastic properties. Yu *et al.*[12] have presented a numerical study on the sedimentation and aggregation of particles in shear–thinning thixotropic fluids, and concluded that the aggregation of two particles settling one above the other is caused by the time–dependent and shear thinning characteristics of the fluid. In addition, it was also observed that the aggregation of randomly distributed particles in such fluids into stable clusters or columns, which is a phenomenon that has been observed in some non–Newtonian fluids (Refs. 13 and 14), requires the suspending fluid to exhibit a degree of elasticity. The dynamics of shear thinning, thixotropic fluids in other systems have been analysed by Derksen,[15] Potanin,[16] and Møller *et al.*[17]

In order to characterise the dependency of the viscous parameters of a fluid on its internal structural network, Gumulya *et al.*[3] utilised a fluid model that is similar to the model of thixotropy proposed by Møller *et al.*[17] The fluid model assumes that the fluid is completely non–elastic. Furthermore, it does not include a constant yield stress value. However, through a series of numerical studies, it was found that the transient response predicted by the model towards a variety of changes in shear conditions (under short time scales) tends to resemble the observed rheological response of typical viscoplastic fluids (Ref. 18).

In this paper, a numerical study of the flow field of a thixotropic, shear thinning fluid surrounding a settling spherical particle will be presented. The utilised numerical method is the Volume–of–Fluid (VOF) method, where the solid particle is likened to a fluid with very high viscosity. While this method is more commonly applied to immiscible fluids with deformable interfaces, the use of VOF to model the movement of a non-deformable material in a fluid domain has previously been examined by Chen *et al.*[19] (in yield–stress fluids), as well as Gumulya[18] (in Newtonian fluids of $Re \leq 4.2$). The apparent agreement shown by Gumulya[18] in the case of a solid particle settling in Newtonian fluids with published experimental data suggests that this method can be used to analyse the flow fields surrounding a particle settling in a fluid domain, without prior knowledge of the drag force experienced by the particle. Further discussion on the validation of this method will be presented in Sec. II B, and the use of this method to analyse the highly coupled and non–linear equations surrounding the settling of a spherical particle in time–dependent non–Newtonian fluids will be examined in this paper. In Sec. II C, the details of the rheology model and its implementation in the VOF framework will be presented. Furthermore, the parameters required for the modelling of the solid particle as a highly viscous fluid will also be discussed (Sec. II D). Section III presents the resulting flow fields and drag force, along with comparisons to relevant experimental data.

II. NUMERICAL MODEL

A. Mathematical formulation and numerical method

Consider an initially stationary metal sphere in a cylinder filled with fluid. The metal sphere exerts a downward shear force on the fluid due to gravitational effects, inducing changes in viscosity and flow in the fluid medium. If the metal sphere is likened to a fluid with very high viscosity (see Sec. II B), this flow problem can be considered to be a dual–phase problem, with the two phases possessing vastly different values of density and viscosity.

Navier–Stokes equations are applied over the whole domain,

$$\nabla \cdot \mathbf{U} = 0, \tag{1}$$

$$\frac{\partial}{\partial \mathbf{t}} (\rho \mathbf{U}) + \nabla \cdot (\rho \mathbf{U}\mathbf{U}) = -\nabla p + \nabla \cdot \boldsymbol{\tau} + \rho \mathbf{g}, \tag{2}$$

where $\mathbf{U}$ is the velocity vector, ρ is the density, p is the pressure, and $\mathbf{g}$ is the gravitational acceleration. The stress tensor $\boldsymbol{\tau}$ is given by

$$\boldsymbol{\tau} = \mu(\dot{\gamma})\dot{\boldsymbol{\gamma}}, \tag{3}$$

where $\dot{\gamma}$ is the second invariant of the rate-of-deformation tensor ($\dot{\boldsymbol{\gamma}}$). At each control volume, the density and viscosity (μ) are

$$\rho = \sum \alpha_q \rho_q, \tag{4}$$

$$\mu = \sum \alpha_q \mu_q, \tag{5}$$

where α_q is the volumetric fraction of the qth phase. In the current study, a value of unity for α indicates that the cell is full of the fluid phase, whereas $\alpha = 0$ indicates that the cell is occupied by the "metal" phase.

In addition, the tendency of the particle to distort from its spherical shape was minimised by the incorporation of a surface tension parameter between the two phases, implemented through the continuum surface force (CSF) model of Brackbill *et al.*,[20]

$$\mathrm{F} = \frac{\rho \sigma \nabla \alpha}{0.5\,(\rho_1 + \rho_2)} \nabla . \left(\frac{\nabla \alpha}{|\nabla \alpha|} \right), \tag{6}$$

where σ is the surface tension coefficient between the "metal" and fluid phases. The magnitude of this coefficient in relation to the viscous and inertial forces in the two phases will be discussed further in Sec. II C.

The flow problem described above was spatially discretised on a two–dimensional axisymmetric numerical grid, which was divided uniformly such that there were 40 control volumes across the diameter of the sphere. An implicit differencing scheme was employed for the temporal discretisation of all the governing equations, whereas the convection terms were discretised using the standard central differencing scheme. The coupled method was adopted for the velocity-pressure coupling in conjunction with the PRESTO (Pressure Staggering Option) scheme for the interpolation for the pressure field in the momentum equation. The resulting equation was implemented into the ANSYS FLUENT 13.0 through a series of user-defined functions (UDFs). Throughout the calculation process, the motion of the sphere was tracked through the Piecewise-Linear Interface Calculation (PLIC) interface–tracking scheme suggested by Youngs.[21] The time step used throughout the calculation process was set such that the global Courant number is less than 0.1.

B. Model validation

The validity of the proposed numerical method was examined through comparisons of the predicted drag force experienced by spheres ($\rho_s = 7638$ kg/m^3; d = 6.25 mm) settling in Newtonian fluids with the representative Stokes drag value. The viscosity of the Newtonian fluid ranges from 0.4 to 5 Pa s, and the fictional surface tension parameter between the two phases was set to 3.5 N/m. The resulting Capillary number $\left(Ca = \mu_f V_t / \sigma\right)$ for these simulations ranges from 0.027 to 0.033. The development of spurious/parasitic currents in the interface of the two phases, which have been known to occur in CSF-based models with considerable imbalance in viscous and surface tension forces (Ref. 22), is therefore expected to be minimal.

The effect of the fictional viscosity parameter for the "solid" material (μ_s) on the development of the flow field around the settling sphere was first examined, based on a fluid viscosity value, μ_f, of 5 Pa s (Figure 1). The settling velocity of the sphere in this case can be seen to be highly

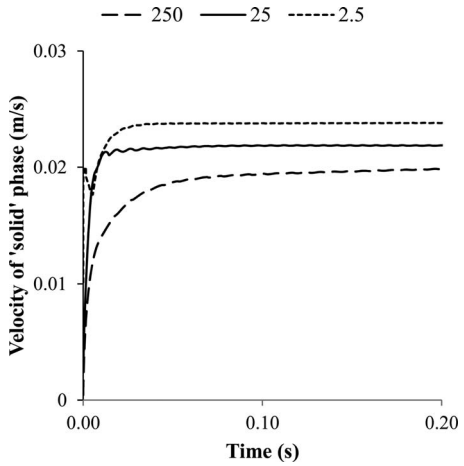

FIG. 1. The development of settling velocity of the "solid" sphere, using several different ratios of μ_s/μ_f. The viscosity of the "fluid" phase is constant (i.e., Newtonian) at 5 Pa s.

dependent on the μ_s value. At higher values of μ_s/μ_f, the development of the velocity field around the sphere tends to be sluggish, as reflected by the lower settling velocity of the sphere at $\mu_s/\mu_f = 250$. With lower μ_s/μ_f values, the development of the velocity field around the sphere was found to be considerably more rapid. However, a velocity overshoot was found in the case where $\mu_s/\mu_f = 2.5$, indicating that the low value of μ_s tends to cause considerable diffusion within the "solid" phase, leading to the formation of a secondary flow within the solid sphere.

The formation of the secondary flow within the "solid" sphere can be inspected further in Figure 2, where the development of the velocity field within the "solid" sphere has been presented. In this figure, it can be seen that while the case with $\mu_s/\mu_f = 250$ presents minimal distribution of velocity within the "solid" phase, the opposite is true with the case where $\mu_s/\mu_f = 2.5$. In the latter case, the diffusion of momentum within the "solid" phase can be seen to cause the velocity distribution within the sphere to be in excess of 20%, with the highest velocity being at the centre of the sphere. The selection of the fictional solid viscosity parameter therefore requires careful consideration of the velocity and flow field development within the two phases. Within the parameters of this study, a μ_s/μ_f ratio of 25 has been found to present a satisfactory balance of rapid flow field development and minimal secondary flow development within the solid phase.

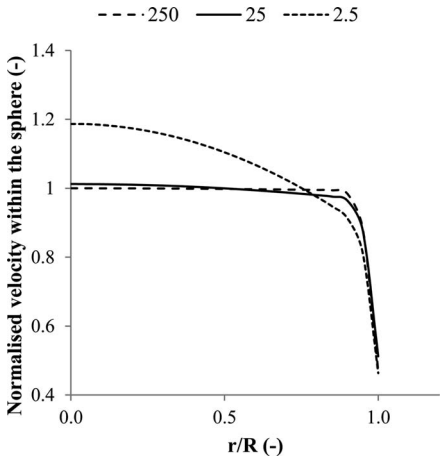

FIG. 2. Magnitude of the velocity field within the "solid" sphere, in a Newtonian fluid ($\mu_f = 5.0$ Pa s). The velocity parameter has been normalised against the average settling velocity of the sphere, and the x axis represents the distance from the centre of the sphere in the radial direction, normalised against the radius of the sphere.

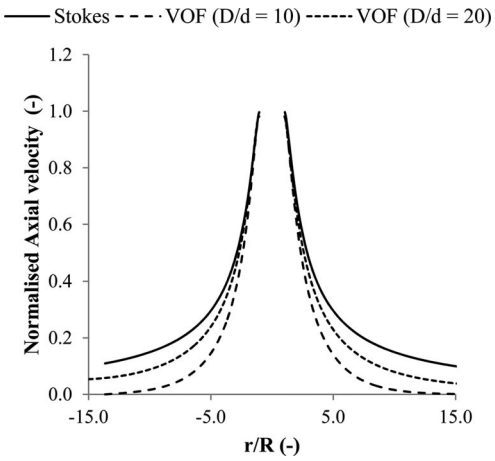

FIG. 3. Axial velocity (normalised against the terminal settling velocity of the sphere) above and below a sphere (d = 6.25 mm) settling in Newtonian fluid (μ_f = 5.0 Pa s) along the axial direction (normalised as distance/sphere radius). D represents the diameter of wall boundary.

The velocity of the fluid surrounding a sphere settling in a 5 Pa s Newtonian fluid has been compared directly with the analytical solution of Stokes (see Figure 3). As expected, the velocity of the fluid tends to decrease with increasing distance from the sphere. Furthermore, the velocity of the fluid medium in a domain where the width of the geometry is 10 times the diameter of the sphere ($D/d = 10$) tends to decrease more rapidly than in the case where $D/d = 20$. The approach of the fluid velocity towards the theoretical Stokes values as the extent of the domain is increased indicates that the discrepancies in the numerical and analytical solution of Stokes have been caused by the extension of the solid wall boundaries in the computational domain.

The resulting drag coefficient experienced by the sphere as presented by the numerical study can be seen in Figure 4. In this figure, the predicted values of drag coefficient (as a function of particle Reynolds number) have been compared against those calculated through the widely accepted correlations of Clift *et al.*[23]. As can be seen in this figure, there is a trend of over-prediction in the numerically predicted drag force, with the predicted values of drag coefficient being approximately 25% higher than the calculated values. This level of discrepancy was as expected, considering that the settling velocity of spheres in cylindrical geometries of diameter 10 times the diameter of the sphere has been found to be approximately 20.8% lower than the theoretical Stokes velocity (Ref. 24). Figure 4 therefore represents an excellent agreement in the theoretical and numerical

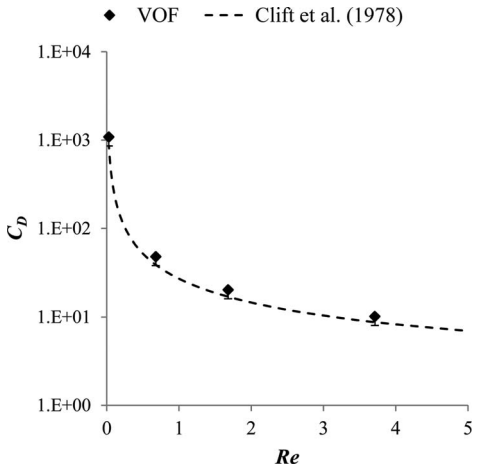

FIG. 4. Drag coefficient surrounding a sphere settling in Newtonian fluids of viscosity $0.4 < \mu_f < 5.0$ Pa s ($D/d = 10$).

TABLE I. Selected fluid and sphere parameters.

Fluids	μ_0 (Pa s)	μ_∞ (Pa s)	$\kappa.\theta$ (s)	m	$V_{t,Newtonian}$ (m/s)	Re	Bn
A	75	0.00089	8.6	0.8	0.0804	0.291	3.8
B	75	0.00089	3.3	1	0.0804	0.291	41.5

predictions of drag force in the flow fields surrounding spheres settling in Newtonian fluids at Reynolds numbers of $Re < 4.0$, indicating the validity of the proposed numerical model.

C. Fluid model

The dependence of fluid viscosity on both shear rate and time is characterised through the incorporation of a scalar variable that represents the structure of the fluid, λ. A fluid medium with a fully intact structure is represented by a λ value of 1.0, whereas a λ value of 0.0 represents a medium where its internal structure has been completely destroyed. Under the assumption that the fluid has a constant characteristic relaxation time, θ, and that the rate of destruction is linearly dependent on the rate of shear, the rate of change in λ could be written:

$$\frac{\partial \lambda}{\partial t} + \mathbf{U} \cdot \nabla \lambda = \frac{1-\lambda}{\theta} - \kappa \dot{\gamma} \lambda, \tag{7}$$

where κ is a constant. Gumulya *et al.*[3] has coupled Eq. (1) with a viscosity equation,

$$\mu = \mu_\infty + (\mu_0 - \mu_\infty)\lambda^m, \tag{8}$$

where μ_0 is the maximum viscosity at zero shear rate and μ_∞ the limiting viscosity at high values of shear rate. As the value of μ_∞ is generally much smaller than μ_0 (see Table I), the viscosity equation can generally be approximated as

$$\mu = \mu_0 \lambda^m. \tag{9}$$

Under steady–state conditions, Eqs. (1) and (2) become

$$\frac{\partial \lambda_{ss}}{\partial t} \to 0 \Rightarrow \lambda_{ss} = \frac{1}{1+\kappa\theta\dot{\gamma}} \tag{10}$$

and

$$\mu = \mu_0 (1+\kappa\theta\dot{\gamma})^{-m}, \tag{11}$$

respectively.

The following set of non-dimensional parameters was incorporated into the analysis of the flow field development surrounding a settling sphere:

$$De = \theta \frac{V_{t,Newtonian}}{d}, \tag{12}$$

$$Re = \frac{\rho_f V_{t,Newtonian} d}{\mu}, \tag{13}$$

where d is the diameter of the sphere, μ is the apparent steady–state viscosity of the fluid, evaluated at a shear–rate of $\left(V_{t,Newtonian}/d\right)$. The parameter $V_{t,Newtonian}$ is the calculated value of terminal settling velocity of a particle settling in a Newtonian fluid. The viscosity of the Newtonian fluid is determined through the steady–state viscosity equation of the thixotropic fluid (see Eq. (11)). De in this case represents the ratio of the time scale of the liquid over the flow time scale. It will be shown in Sec. III that the viscosity distribution around the settling sphere, and hence the drag force and terminal settling velocity of a particle settling in shear–thinning thixotropic fluids is highly dependent on the relaxation time of the fluid.

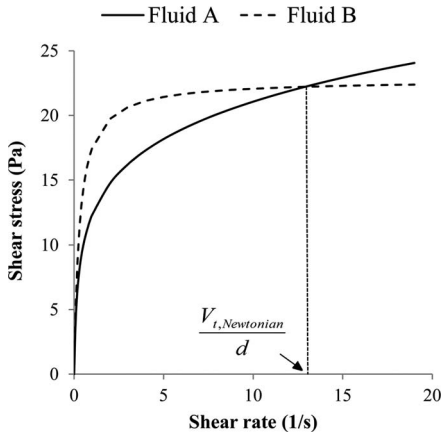

FIG. 5. Steady-state rheology (see Eq. (10)) and the evaluation of τ_Y.

Another dimensionless parameter was needed to describe the rheological properties of the fluid:

$$Bn = \frac{\tau_Y d}{\eta V_{t,Newtonian}}. \tag{14}$$

Bn is the pseudo–Bingham number that signifies the ratio of the pseudo–yield stress of the fluid (if its rheogram was interpreted as a Bingham fluid, see Figure 5) to the actual viscous parameters of the study. The parameter η represents the gradient of the steady–state rheogram, evaluated at the characteristic shear rate value. The pseudo yield stress τ_Y is evaluated by extrapolating the shear behaviour at the characteristic shear conditions to $\dot{\gamma}$ value of 0.

Based on the considerations stated above, a set of parameters were selected for the rheological properties of the fluids (see Table I). In all of the simulations, the density and diameter of the ball were set to 7638 kg/m^3 and 6.25 mm, respectively, and the density of the fluid medium was 998 kg/m^3. The distance of the centre of the sphere to the wall boundary is 62.5 mm. An initial value of λ of 1.0 is used to represent a completely undisturbed fluid medium, whereas its value within the "metal" sphere is 0.0. The simulations were carried out until a steady–state solution is obtained, i.e., until the sphere reaches a steady settling velocity.

D. Numerical parameters

Based on the results of the numerical study with Newtonian fluids, a solid viscosity parameter of 25 times the maximum viscosity of the fluid has been selected throughout all the study with the thixotropic, shear-thinning fluids. The effect of the fictional parameter of surface tension between the two phases can be inspected in Figure 6, where the deformation of the spheres at 3 different values of σ has been presented. As can be seen in this figure, $\sigma = 0.35$ N/m (Figure 6(a)) imparted significant deformation in the sphere. On the other hand, at $\sigma = 3.5$ N/m, the deformation of the sphere as it settles down through the shear-thinning fluid can be seen to be minimal. As can be expected, lower levels of sphere deformation are obtained, as the "surface tension" between the two phases is increased.

The effect of the surface tension force as the σ parameter is increased further from 3.5 N/m can be seen in Figure 7, where the development of velocity field surrounding the sphere for cases where $\sigma = 1.0$, 3.5, and 10 N/m has been presented. It can be seen that although the velocity fields below the sphere are very similar across the 3 cases, considerable differences are evident with the flow field above the settling sphere. In the case of $\sigma = 10$ N/m, a significant overshoot in velocity tends to occur immediately downstream of the sphere. This could be caused by the development of spurious/parasitic currents, which have been known to occur in CSF-based models with considerable imbalance in viscous and surface tension forces (Ref. 20). In the region above the sphere, the value of

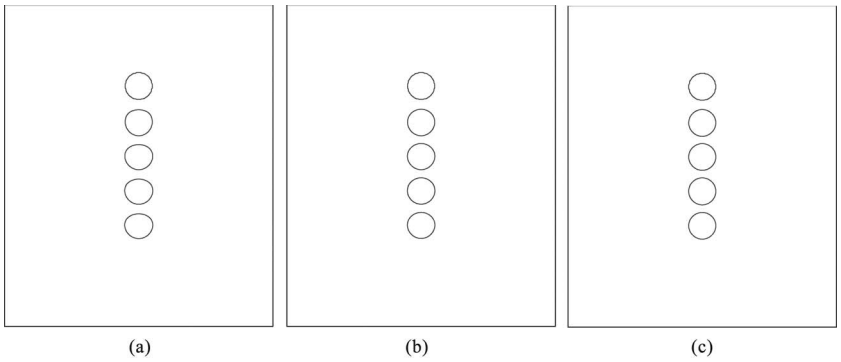

FIG. 6. The deformation of the sphere in fluid of Case A, with De = 128 (see Table I): (a) $\sigma = 0.35$ N/m ($Ca = 0.295$); (b) $\sigma = 1.0$ N/m ($Ca = 0.103$); (c) $\sigma = 3.5$ N/m ($Ca = 0.0295$).

λ is considerably lower than 1.0, and therefore the viscosity of the fluid in this region is significantly lower than that below the sphere.

A fictional surface tension parameter of 3.5 N/m has therefore been selected for all of the simulations conducted for this study. The resulting range of Capillary numbers $\left(Ca = \left(\mu_f V_{t,Newtonian}\right)/\sigma\right)$ for Fluids A and B was 0.0295–0.033, which is consistent with the range of Capillary numbers selected for the study with the Newtonian fluids.

A series of grid independence tests was conducted to determine the convergence of the current numerical problem. The results of this study are presented in Figure 8, where the development of sphere settling velocity over time has been shown for cases using *d*/20, *d*/40, and *d*/80 numerical grids. As can be seen, the case with *d*/40 numerical mesh tends to approach the results of *d*/80, indicating that a grid independent result has been obtained. A numerical grid of *d*/40-sized cells was thus selected for this study.

III. RESULTS AND DISCUSSION

For particles settling in shear–thinning, thixotropic fluids, the development of drag force surrounding it is expected to be highly dependent on the rates of deformation and reconstitution of the fluid structural parameter, i.e., the response time of the fluid, which in this study is characterised by *De*. This is shown in Figure 9, where the development of settling velocity of a particle in Case A fluids with different *De* values has been presented. As expected, the time required for the particle

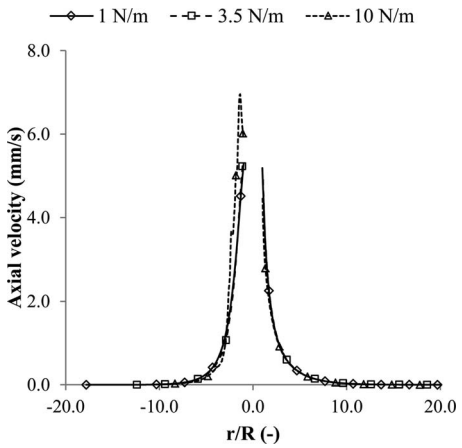

FIG. 7. Axial velocity above and below the sphere along the axial direction (normalised as distance/d), using $\sigma = 1.0$, 3.5, and 10 N/m (Case A, De = 28.2, see Table I).

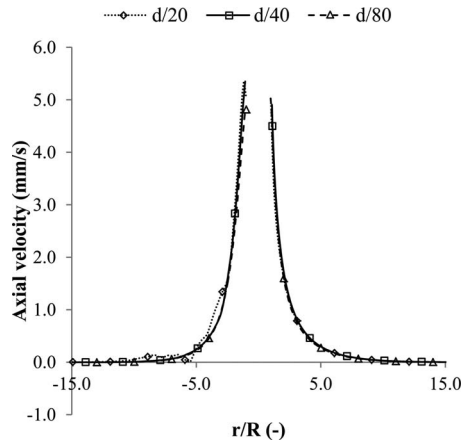

FIG. 8. Normalised axial velocity above and below the sphere along the axial direction (normalised as distance/*d*), using *d*/20, *d*/40, and *d*/80 numerical grids (Case A, $De = 28.2$, see Table I).

to achieve a terminal settling condition increases with increasing values of *De*. Furthermore, the terminal settling velocity in the thixotropic fluids appears to be inversely proportional to *De*. As will be shown later, this is due to the distribution of apparent viscosity surrounding the sphere, which tends to become more localised as the *De* value is increased. This is consistent with the findings of Derksen,[15] who found that the drag force experienced by random particles suspended in thixotropic suspensions tends to increase with increasing fluid response time.

The distribution of λ around particles settling in fluids of Case A has been presented in Figure 10. These figures were obtained in cases where the particles have reached their respective terminal settling velocities, such that they represent the steady–state flow fields of the fluids. It can be seen that the distribution of λ, and hence viscosity, around the particles depends greatly on the *De* value of the fluid. Fluids with shorter response times (Figures 10(b)–10(d)) tend to have greater areas of disturbance (i.e., fluid regions with low viscosity) in comparison to fluids with the higher values of θ (Figure 10(a)). This is especially pronounced in areas immediately surrounding the sphere. A particle settling through a fluid with $De = 561$ (Figure 10(a)) thus experiences a greater viscous resistance and drag force in the flow field immediately surrounding it in comparison to a particle settling in fluids with lower *De* values. This is reflected by the terminal settling velocity of the particles, which has been shown to decrease with increasing values of *De* (see Figure 9).

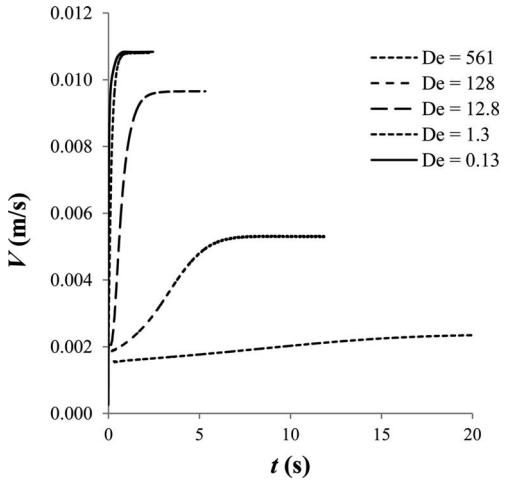

FIG. 9. The development of settling velocity of a sphere ($d = 6.25$ mm, $\rho_s = 7368$ kg/m^3) in Case A fluids of different *De* values as a function of time.

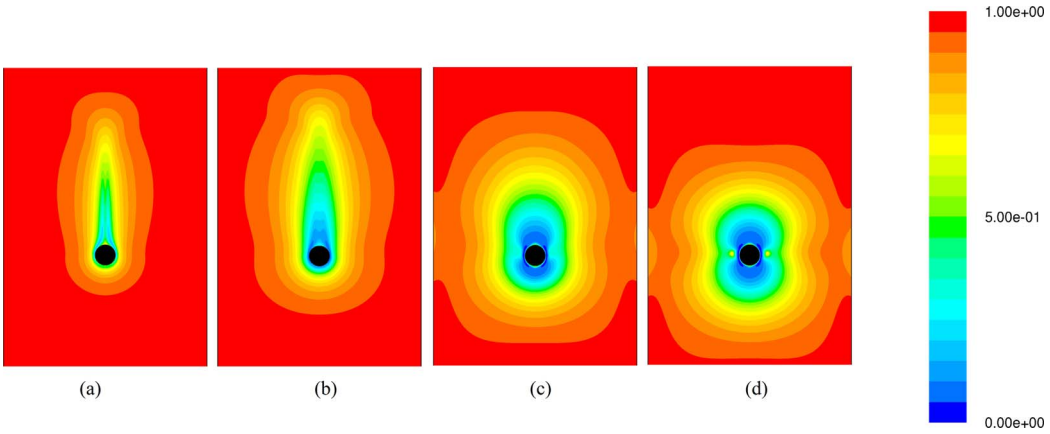

FIG. 10. Contours of the fluid structural parameter (λ) in Case A fluids: (a) $De = 560$; (b) $De = 128$; (c) $De = 12.8$; (d) $De = 1.3$.

Figure 10 also shows that in cases with higher values of *De*, strong fore–aft asymmetry tends to be developed around the settling spheres. In the case of the fluid presented in Figure 10(d), the *De* value ($De = 1.3$) is in the same order as the characteristic time scale of the experiment ($t^* = 1/\dot{\gamma} = 0.58$, with $\dot{\gamma}$ being evaluated at the terminal settling velocities of the spheres), and highly symmetrical flow field is obtained in the fore–aft region of the sphere. On the other hand, in the case of the fluid presented in Figure 10(a), the value of *De* ($De = 561$) is much larger than $t*$. The flow field in this case shows the formation of a "tail," where the structure of the fluid gradually recovers after being sheared by the movement of the sphere.

The fore–aft asymmetry in the flow fields can be inspected further in Figure 11, where the axial distribution of λ for cases of fluids with different *De* values has been presented graphically. In the region below the settling sphere, the extent of structural disruption caused by the movement of the settling sphere (represented by fluid regions where $\lambda < 1.0$) increases steadily with decreasing values of *De*. On the other hand, in the region above the settling sphere, the values of λ tend to decrease with increasing De values, caused by the delayed recovery of the fluid after being sheared by the moving sphere. The asymmetry in the regions above and below the sphere is especially apparent in cases where the *De* value of the fluid is high ($De = 128$ and $De = 561$). While the fluid with $De = 561$ appears to have higher values of λ above the sphere in comparison to the fluid with

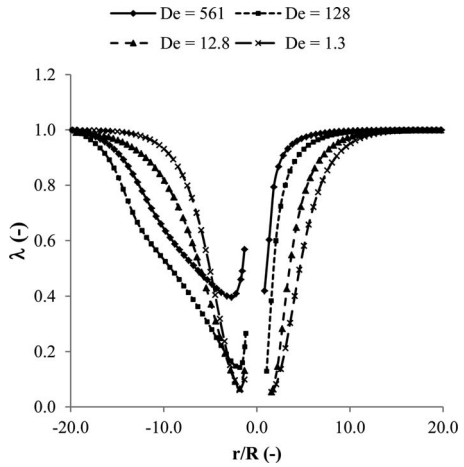

FIG. 11. Axial profile of the structural parameter (λ) in Case A fluids with different *De* values. The distance parameter presented in the x axis was normalised against the radius of the sphere. Negative distance values indicate regions above the settling sphere, and vice versa.

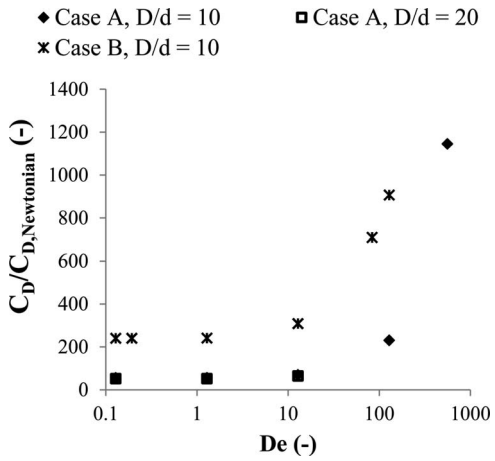

FIG. 12. Drag coefficient (normalised against the C_D value of a sphere settling in a Newtonian fluid, calculated through the Stokes C_D-Re relation) experienced by a sphere settling in Case A and Case B fluids of different De values. The distance to the wall boundary relative to the diameter of the sphere is also varied (D/d = 10 and D/d = 20).

$De = 128$, this could be caused by the increased drag force of the fluid at $De = 561$, resulting in a lower level of structural destruction in the fluid. The fluid in this region thus appears to recover faster than in the case of $De = 128$.

In Figure 10, it appears that the area of disturbance surrounding spheres settling in fluids of $De \leq 12.8$ is relatively large in comparison to the computational domain. The effects of the wall boundaries on the velocity development around the sphere in fluids of different *De* values therefore needed to be examined. This was conducted through simulations of larger geometries, in which the distance of the wall boundary to the sphere centre is 20 times the diameter of the sphere ($D/d = 20$). The results of this analysis have been presented in Figure 12, where the values of the drag coefficient have been presented as a function of the *De* value of the fluid. The C_D values in this case have been normalised against the drag coefficient of a sphere settling in a Newtonian fluid with a viscosity value equal to the steady–state viscosity of a thixotropic, shear–thinning fluid evaluated at a shear–rate of $\left(V_{t,Newtonian} / d\right)$.

In Figure 12, it is evident that despite the fact that the areas of disruption surrounding the sphere for cases where $De = 12.8$ and $De = 1.3$ are large in comparison to the size of the domain (this occurs to the extent that the values of λ on the wall boundary at $D/d = 10$ is less than 1.0), the effects of the boundary on the development of the flow field are relatively minimal in comparison to cases involving Newtonian fluids. In Case A fluids, the difference in the C_D values of spheres settling in columns with *D/d* values of 10 and 20 were found to be less than 8%. The minimal difference in the drag coefficient of the spheres could be caused by the considerable shear thinning properties of the fluid, where the localisation of the fluid viscosity is quite severe, such that the presence of wall boundaries surrounding the sphere/fluid configuration does not greatly influence the drag force experienced by the spheres.

Figure 12 also shows that the values of C_D for spheres settling in Fluid B are considerably higher than those settling in Fluid A. This was as expected, due to the fact that Fluid B has a higher *Bn* value than Fluid A. This is such that while the viscosity of the two fluids $\left(\mu = \tau / \dot{\gamma}_{ref}\right)$ at the reference value of $\dot{\gamma}_{ref} = V_{t,Newtonian} / d$ is the same for Fluids A and B (see Figure 5), the apparent viscosity ($\eta = \delta\tau / \delta\dot{\gamma}$) of the two fluids differ considerably. Fluid regions away from the surface of the sphere would therefore require higher values of shear stress to reduce the structural parameter of Fluid B in comparison to Fluid A, resulting in a higher level of flow field localisation in the case of the fluid with the higher *Bn* value.

The effects of the *Bn* values on the flow field surrounding a settling sphere can be seen in Figure 13, where the contours of the second invariant of the strain-rate tensor in fluids of Cases A ($Bn = 3.8$) and B ($Bn = 41.5$) have been presented. The strain rate parameter has been normalised

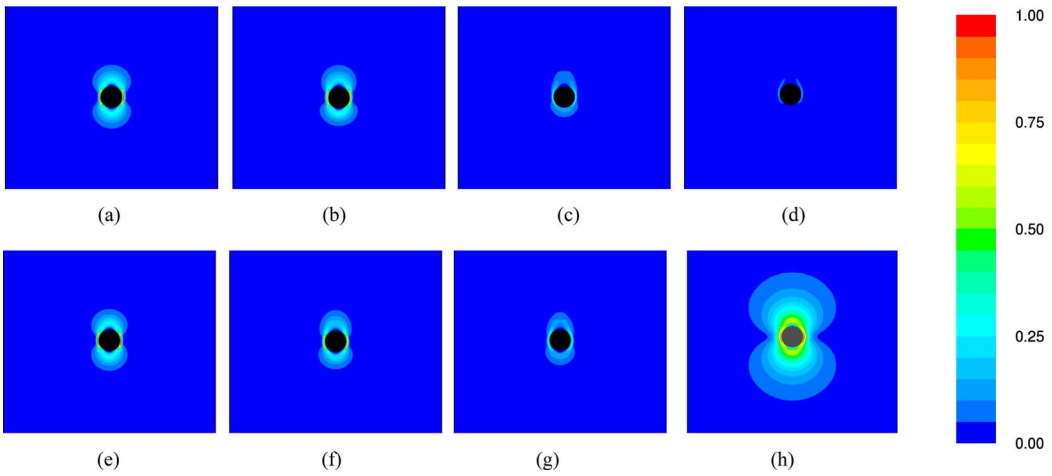

FIG. 13. Contours of the second invariant of the strain-rate tensor. The magnitude of the strain-rate tensor was normalised against the maximum strain rate value obtained as the De value reaches 0.13 for cases of non-Newtonian fluids ((a)–(g)). For the case of the Newtonian fluid (1.725 Pa s), the magnitude of the strain-rate tensor was normalised against the maximum strain rate value (h).

against a maximum strain rate value, which is characteristic of the rheological parameters of the fluid. In the present study, it was found that there is minimal difference (0.6%) in the C_D values of Cases A and B fluids with *De* values of 1.3 and 0.13. It was therefore concluded that the minimum drag coefficient, and hence maximum strain rate value, could be estimated using the flow fields resulting from cases of $De = 0.13$ for both of Fluids A and B.

The fluid medium represented in Figure 13(h) is Newtonian with a *Bn* value of zero. The area of deformation in the case of the Newtonian fluid can be seen to be significantly larger than in the cases of the thixotropic, shear-thinning fluids. Away from the surface of the sphere, the rate of strain experienced by the Newtonian fluid decreases gradually. Shear rate values of less than 0.1 s^{-1} is reached at a distance of ∼3 times the diameter of the sphere in the axial direction. In the radial direction, the extension of the flow field spans ∼4 times the diameter of the sphere.

On the other hand, the flow fields of the thixotropic, shear–thinning fluids in Figures 13(a)–13(g) appear to have distinct areas of sheared fluid, surrounded closely by regions where the shear rate is close to zero. Fluid B, which has a higher *Bn* value than Fluid A, appears to have slightly smaller area of sheared fluid around the spheres in comparison to Fluid A. In both cases, the regions of sheared fluid extend approximately the 1.25–3 times diameter of the particle in the axial direction, beyond which the shear rate in the fluid decreases rapidly to values lower than 0.1 s^{-1}. In the radial direction, the extension of the flow field is even more restricted, spanning ∼1.25–2 times the diameter of the sphere.

The effects of *Bn* on the flow fields surrounding the spheres can be inspected further in Figure 14, where the profiles of the fluid structural parameter (λ) as a function of the axial and radial distance from the sphere (normalised against the radius of the sphere) have been presented. In the case of Fluid B, the values of λ can be seen to increase at a greater rate, with increasing values of r/R, in comparison to the case of Fluid A. This was as expected, as the higher value of *Bn* in the case of fluid B means that higher values of shear stress would be required to overcome the structural parameter of the fluid. The extension of the flow field surrounding the sphere therefore decreases with increasing values of *Bn*.

Within the area of deformation, a torus of fluid is formed in the lateral direction, translating with the settling movement of the sphere. Such formation has previously been hypothesised by Beris *et al.*[4] in yield–stress fluids, attributed towards the rigid–body rotation of the fluid in regions between the high–shear zones at the sides of the sphere and the recirculation zone further away from the sphere. In the current study, although such rigid–body motion is not possible (due to the lack of a constant yield–stress parameter in the fluid model), the formation of the torus can be explained in

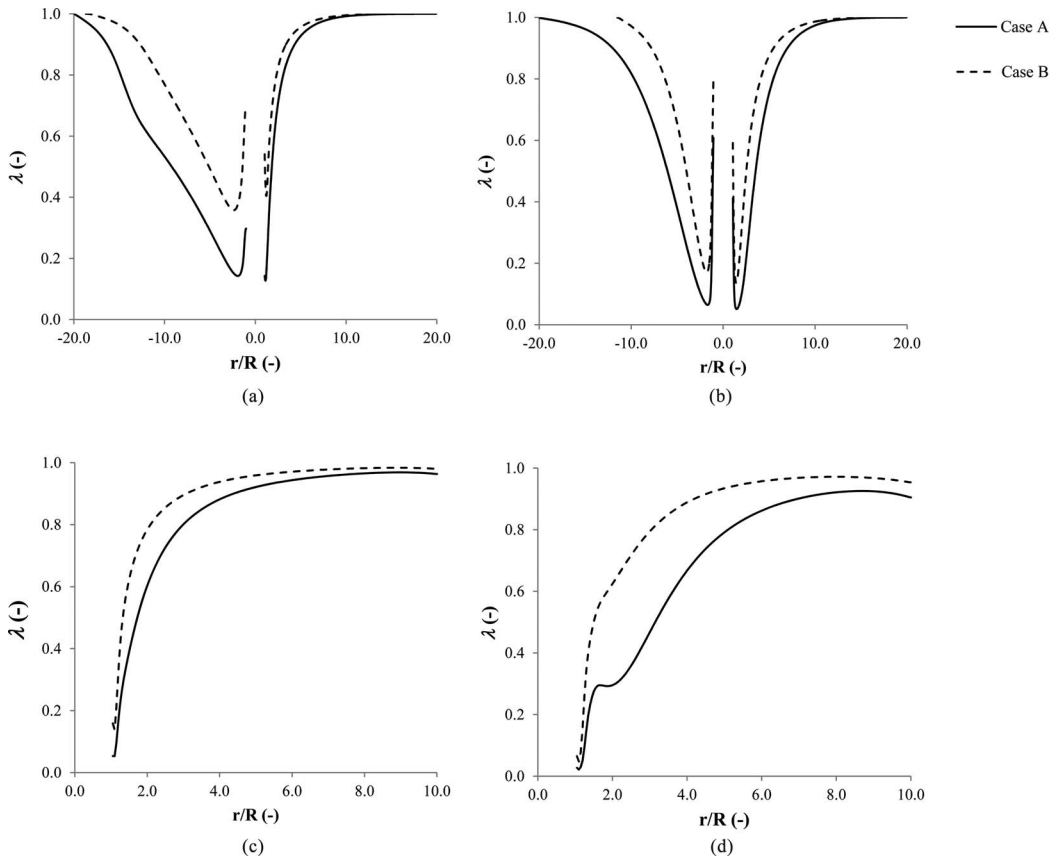

FIG. 14. Profile of the structural parameter (λ) in fluids of Cases A and B: (a) Axial distribution in fluids with De = 12.8; (b) axial distribution in fluids with De = 1.3; (c) radial distribution in fluids with De = 12.8; (d) radial distribution in fluids with De = 1.3. The distance parameter presented in the x axis was normalised against the radius of the sphere. Negative distance values in (a) and (b) indicate regions above the settling sphere, and vice versa.

a similar manner, i.e., fluids in regions away from the high–shear zones at the sides of the sphere do not experience shear stresses that are sufficient to overcome the viscosity of the fluid and further reduce its structural parameter. This results in a slight rotational flow in the area just outside of the high–shear zone, causing the onset of the recirculation zone to appear closer to the edge of the sphere in comparison to the flow fields in Newtonian fluids. The development of the recirculation zone around the settling sphere can be seen in Figure 15.

The asymmetry of the flow field surrounding the settling spheres in Figures 10 and 11, and 13–15 can be compared to the results of the flow visualisation experiments of Gueslin *et al.*,[9,10] who conducted their experiments in colloidal suspensions of clay, which has previously been identified

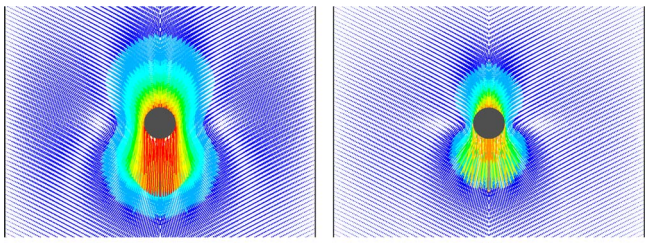

FIG. 15. Velocity fields for a sphere settling in (a) Newtonian fluid of 1.725 Pa s viscosity; (b) Fluid A ($Bn = 3.8$; $De = 128$).

to exhibit yield stress, shear thinning, and "aging" characteristics. Most notably, the velocity field presented in Figure 15(b) can be seen to be in excellent agreement to the velocity fields surrounding an aluminium particle settling in clay suspension (Ref. 9), which also features a strong asymmetry in the fore-aft region of the sphere.

On the other hand, Gueslin *et al.*[9,10] also found that there is a tendency for the downstream flow field to form a "negative wake," i.e., a region of fluid where the fluid velocity is negative with respect to the direction of the settling sphere. This was found in cases where a heavier particle is used (Ref. 9) and/or in cases where the fluid is allowed to "age" prior to the commencement of the experiment (Ref. 10). Interestingly, it was shown that the development of negative wake in the case of aging clay suspensions tends to occur only in cases where the fluid is rested for 2 h or more. In cases where the resting times are less than 2 h, the flow fields surrounding the settling sphere were found to be comparable to that presented in Figure 15(b). Similarly, Putz *et al.*[11] also found that Carbopol solutions, which are traditionally considered as yield–stress fluids, tend to form negative wakes in the area downstream of a settling sphere. The development of negative velocity could not be reproduced in the present study due to the assumption of negligible elasticity in the fluid model.

The implication of the flow fields described above concerns the drag force experienced by particles settling in partially recovered domain. In experiments involving spheres settling one after the other in the same flow path, for example, it is expected that the following sphere, which settles through a partially recovered fluid structure, exhibits a higher settling velocity than the preceding sphere. This phenomenon has previously been observed in several yield–stress and shear thinning fluids (Refs. 3, 14, 25, and 26). In Figure 16, the variability of the second invariant of the strain-rate tensor in fluid A (with $De = 128$) around a sphere settling through a partially recovered domain (the case of the "second sphere") has been presented. In this case, the fluid was previously disrupted by the movement of an earlier ("first") sphere, with a time lapse of 5.8 s. Through this figure, it is evident that the area of disturbance around the settling sphere is now slightly larger than in the case of a sphere settling through an undisrupted fluid domain, indicating that the drag force experienced by the second sphere is lower than that experienced by the earlier sphere. The current finding is therefore consistent with these experimental observations.

The dependency of the drag force experienced by a sphere settling in partially recovered domain on the recovery time of the fluid can be inspected in Figure 17, where the drag coefficient of the "second sphere," normalised against the drag coefficient of a sphere settling in a fully reconstituted domain ($C_{D,1}$), has been presented. As can be expected, the drag coefficient of the second sphere was found to be considerably lower than that of the first sphere, and this parameter decreases with lower values of Δt. Interestingly, in cases where the recovery time of the fluid is almost twice the

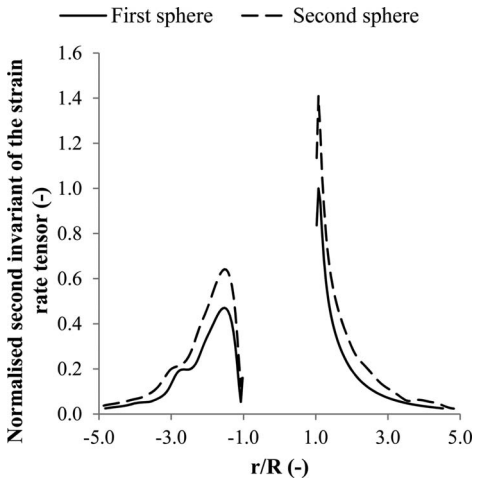

FIG. 16. Second invariant of the strain tensor around two spheres settling one above the other, normalised against the maximum strain rate of the first sphere, along the axial direction (normalised as distance/r). Case A fluid with *De* value of 128 was used, and the first sphere passes through the fluid domain 5.8 s before the movement of the second sphere.

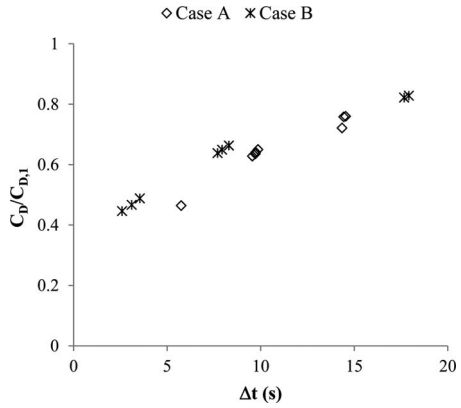

FIG. 17. Drag coefficient of a sphere settling in the same pathline as another sphere. The time difference presented in the x–axis denotes the time lapse since the first sphere passes through the current position of the second sphere. The drag coefficient of the second sphere was normalised against the drag coefficient of the first sphere. The *De* value of fluids A and B were 128.

value of its relaxation time (De = 128, or θ = 10 s for both Fluids A and B), the drag coefficient of the sphere can be seen to still be approximately 20% lower than the drag coefficient of a sphere settling under terminal (or fully reconstituted) conditions. The full recovery of a thixotropic, shear thinning fluid may therefore be considerably longer than the relaxation parameter of the rheology model.

The results of this study highlight the importance of considerations of timeframes and fluid relaxation times in studies involving the drag force and dynamics of particles settling in highly shear thinning fluids. The fluid relaxation time influences the localisation of the viscosity field around the sphere, thus affecting the drag force and the terminal settling velocity, even when the sphere is settling through a fluid domain with a completely intact structure. In partially recovered domains, as the development of viscosity field is highly affected by the fluid structure parameter, lower levels of drag forces are developed around the settling sphere, and hence its settling velocity would be higher than a sphere settling through a fully structurally intact fluid domain. While full reconstruction of the flow fields obtained through flow visualisation experiments was still unachievable (mainly due to the assumption of negligible fluid elasticity in the fluid model), the resulting flow fields can be seen to provide a closer representation of the actuality of shear-thinning, thixotropic fluids and the variability of rheological parameters with time. Future studies will further address the variability of drag force of the particles with the rheological parameters of the fluid.

IV. CONCLUSION

A numerical analysis has been presented, through which the gradual destruction and recovery of the micro–structural properties of a fluid as it is sheared by the movement of a sphere can be emulated. Due to the highly shear thinning characteristics of the fluid, distinct regions of disturbed and undisturbed fluid were formed around the settling sphere, resulting in a localisation of flow field around the sphere. The extent of this localisation is highly dependent on the fluid relaxation time. Fluids with high values of relaxation time tend to develop highly localised shear region around the sphere, causing the sphere to inhibit a greater value of drag force in comparison to spheres settling in fluids with shorter relaxation times. Further, the drag force experienced by the sphere was also found to be highly dependent on the shear thinning characteristics and apparent viscosity of the fluid, which further determines the gradients of strain rate in the flow field surrounding the sphere.

The gradual recovery of the fluid after being sheared by the movement of a sphere tends to cause the region above the sphere to exhibit lower values of viscosity. The flow fields above and below the settling sphere are therefore highly asymmetrical. Such asymmetry was found to be in relative agreement with the results of the flow visualisation experiments of Gueslin *et al.*,[9] although

some discrepancies exist due to the assumption of negligible elasticity in the current fluid model. As a result of this gradual recovery, a sphere that settles through a partially recovered domain, e.g., due to the motion of an earlier sphere, would tend to attain a greater settling velocity than the terminal velocity value. This finding was found to be consistent to several experimental observations conducted in highly shear thinning fluids with time–dependent characteristics, whereby under short time scales, the fluids may be interpreted using yield-stress models.

ACKNOWLEDGMENTS

M.M.G. and V.P. wish to acknowledge Professor Horsley for his supervision, directions, and support to this research.

[1] R. P. Chhabra, *Bubbles, Drops, and Particles in Non-Newtonian Fluids* (CRC Taylor & Francis, Boca Raton, FL, 2007).
[2] M. M. Gumulya, R. R. Horsley, and K. C. Wilson, "The settling of consecutive spheres in viscoplastic fluids," Int. J. Min. Proc. **82**, 106 (2007).
[3] M. M. Gumulya, R. R. Horsley, K. C. Wilson, and V. Pareek, "A new fluid model for particles settling in a viscoplastic fluid," Chem. Eng. Sci. **66**, 729 (2011).
[4] A. N. Beris, J. Tsamopoulos, R. C. Armstrong, and R. A. Brown, "Creeping motion of a sphere through a Bingham plastic," J. Fluid Mech. **158**, 219 (1985).
[5] J. Blackery and E. Mitsoulis, "Creeping motion of a sphere in tubes filled with a Bingham plastic material," J. Non–Newtonian Fluid Mech. **70**, 59 (1997).
[6] M. Beaulne and E. Mitsoulis, "Creeping motion of a sphere in tubes filled with Herschel–Bulkley fluids," J. Non–Newtonian Fluid Mech. **72**, 55 (1997).
[7] B. T. Liu, S. J. Muller, and M. Denn, "Convergence of a regularization method for creeping flow of a Bingham material about a rigid sphere," J. Non–Newtonian Fluid Mech. **102**, 179 (2002).
[8] B. Deglo de Besses, A. Magnin, and P. Jay, "Sphere drag in a viscoplastic fluid," AIChE J. **50**, 2627 (2004).
[9] B. Gueslin, L. Talini, B. Herzhaft, Y. Peysson, and C. Allain, "Flow induced by a sphere settling in an aging yield-stress fluid," Phys. Fluids **18**, 103101 (2006).
[10] B. Gueslin, L. Talini, and Y. Paysson, "Sphere settling in an aging yield stress fluids: Link between the induced flows and the rheological behavior," Rheol. Acta **48**, 961 (2009).
[11] A. M. V. Putz, T. I. Burghelea, I. A. Frigaard, and D. M. Martinez, "Settling of an isolated spherical particle in a yield stress shear thinning fluid," Phys. Fluids **20**, 033102 (2008).
[12] Z. Yu, A. Wachs, and Y. Peysson, "Numerical simulation of particle sedimentation in shear-thinning fluids with a fictitious domain method," J. Non-Newtonian Fluid Mech. **136**, 126 (2006).
[13] G. Gheissary and B. H. A. A. van den Brule, "Unexpected phenomena observed in particle settling in non-Newtonian media," J. Non-Newtonian Fluid Mech. **67**, 1 (1996).
[14] M. M. Gumulya, R. R. Horsley, V. Pareek, and D. D. Lichti, "The effects of fluid viscoelasticity on the settling behaviour of horizontally aligned spheres," Chem. Eng. Sci. **66**, 5822 (2011).
[15] J. J. Derksen, "Drag on random assemblies of spheres in shear-thinning and thixotropic liquids," Phys. Fluids **21**, 083302 (2009).
[16] A. Potanin, "3D simulations of the flow of thixotropic fluids, in large–gap Couette and vane–cup geometries," J. Non–Newtonian Fluid Mech. **165**, 299 (2010).
[17] P. C. F. Møller, J. Mewis, and D. Bonn, "Yield stress and thixotropy: On the difficulty of measuring yield stresses in practice," Soft Matter **2**, 274 (2006).
[18] M. M. Gumulya, "The settling of spheres in viscoplastic fluids" Ph.D. thesis (Curtin University of Technology, 2010).
[19] L. Chen, J. A. Reizes, E. Leonardi, and Y. Li, "Ball falling through viscoplastic fluid in a cylinder," in *Proceedings of the 13th Australasian Fluid Mechanics Conference*, edited by M. C. Thompson and K. Hourigan (Monash University – Department of Mechanical Engineering, Victoria, 1998), p. 297.
[20] J. U. Brackbill, D. B. Kothe, and C. Zemach, "A continuum method for modeling surface tension," J. Comput. Phys. **100**, 335 (1992).
[21] D. L. Youngs, "Time-dependent multi-material flow with large fluid distortion," in *Numerical Methods for Fluid Dynamics*, edited by K. W. Morton and M. J. Baines (Academic Press, New York, 1982), pp. 273–285.
[22] D. J. E. Harvie, M. R. Davidson, and M. Rudman, "An analysis of parasitic current generation in volume of fluid simulations," ANZIAM J. **46**(E), C133–C159 (2005).
[23] R. Clift, J. R. Grace, and M. E. Weber, *Bubbles, Drops, and Particles* (Academic Press, Inc., London, 1978).
[24] W. L. Haberman and R. M. Sayre, "Wall effects for rigid and fluid spheres in slow motion with a moving liquid," David Taylor model Basin Report No. 1143, Washington D.C., 1958.
[25] M. R. Horsley, R. R. Horsley, and K. C. Wilson, "Non-Newtonian effects on fall velocities of pairs of vertically aligned spheres," J. Non-Newtonian Fluid Mech. **124**, 147 (2004).
[26] M. Hariharaputhiran, R. S. Subramanian, G. A. Campbell, and R. P. Chhabra, "The settling of spheres in a viscoplastic fluid," J. Non-Newtonian Fluid Mech. **79**, 87 (1998).